Preparation and characterization of CrN_xO_y thin films: the effect of composition and structural features on the electrical behavior

R Arvinte[1,2], J. Borges[1], R. E. Sousa[1], D. Munteanu[2], N.P. Barradas[3], E. Alves[3], F. Vaz[1], L.Marques[1]

[1]Departamento/Centro de Física, Universidade do Minho, 4710-057 Braga, Portugal

[2]Dept. of Technological Equipment and Materials Science, Transilvania University, 29 Eroilor Blvd., 500036 Brasov - Romania

[3]Departamento de Física, Instituto Tecnológico Nuclear, E.N. 10, 2686-953 Sacavém, Portugal

Abstract

Metallic oxynitrides have attracted the attention of several researchers in the last decade due to their versatile properties. Through the addition of a small amount of oxygen into a transition metal nitride film, the material's bonding states between ionic and covalent types can be tailored, thus opening a wide range of electrical, optical, mechanical and tribological responses. Among the oxynitrides, chromium oxynitride (CrN_xO_y) has many interesting applications in different technological fields. In the present work the electrical behavior of CrN_xO_y thin films, deposited by DC reactive magnetron sputtering, were investigated and correlated with their compositional and structural properties. The reactive gas flow, gas pressure, and target potential were monitored during the deposition in order to control the chemical composition, which depend strongly on reactive sputtering process. Depending on the particular deposition parameters that were selected, it was possible to identify three types of films with different growth conditions and physical properties. The electrical resistivity of

the films, measured at room temperature, was found to depend strongly on the chemical composition of the samples.

Keywords: magnetron sputtering, electrical resistivity, chromium oxynitride

1. Introduction

Thin film technology has been applied with enormous success in several technological fields, such as solar cells/collectors, optical devices for UV-visible spectral region applications, colored layers, automotive parts, barrier and insulating layers in electronic devices, providing unique benefits in terms of lifetime and performance. In terms of specific examples of synthetic materials used in the above mentioned applications, the transition metal oxide thin films, MeO_x, are frequently applied in optical devices, such as anti-reflection and dense wavelength multiplexing devices and switchable windows [1-3]. These applications are enabled by the excellent mechanical properties of oxide-based films together with a good chemical stability, high index of refraction and wide optical band gap, high electrical resistivity and dielectric constant. On the other hand, transition metal nitrides such as ZrN, TiN and HfN are used as refractory compounds. They exhibit a wide number of exceptional physical properties, including their relatively high hardness, high melting point, chemical stability and corrosion resistance [4]. These properties are related with the binding mechanism, which comprises three bonding types: metallic, covalent and ionic [5,6]. Combining these two alloys gives rise to a new class of materials, the oxynitrides, MeO_xN_y (Me = early transition metal). The ternary alloys are gaining importance in several technological applications [7-12] due to the possibility to tune the properties between those of metallic nitrides, MeN, and those of the correspondent insulating oxides, MeO_x, by changing the O content. Balancing the oxide/nitride ratio allows us to tune the band-gap and

crystallographic order between oxide and nitride and hence the electronic and optical properties of the oxynitride alloy.

Of particular interest is CrO_xN_y due to the importance of their nitrides and oxides in a number of technological applications [13-16]. In fact CrN has excellent mechanical properties, oxidation resistance, chemical stability, it has been used as a material for cutting tools, plastic metal moulds, and frictional parts [17]. It also finds applications in automotive industry as coatings for lubricated tribological systems. They are also used in moulds and pins for aluminium die casting, where mechanical resistance and high temperature oxidation resistance is required [18]. Also, Cr_2O_3 is very stable under ambient conditions and it is characterized by its chemical inertness, stability, mechanical strength and relatively high hardness. Previous research shows that the hardness of chromium oxide coatings strongly depends on the stoichiometric polycrystalline Cr_2O_3 phase present in the coating [19], with high quality Cr_2O_3 stoichiometric coatings reaching nearly 30 GPa hardness combined with good scratch resistance. In terms of optical-based applications, Cr_2O_3 thin films include electrochromic coatings, infrared (IR)-transmitting coatings, selective black absorbers, and optically selective surfaces of solar collectors [20]. As chromium oxide is an insulating antiferromagnetic material it is also suitable as a tunnel junction barrier [21].

Depending on its stoichiometry CrN_x shows a metallic-like ($\rho_{CrN} \approx 6.4\times10^{-4}$ Ω cm, $x \approx 0.93$) or semiconducting behaviour ($\rho_{CrN} > 1\times10^{-2}$ Ω cm, $x \approx 1.06$), while chromium oxide is a insulator ($E_g \approx 4$ eV, $\rho_{Cr2O3} >> 1$ Ω cm). Combining both materials as chromium oxynitride opens the possibility to tune the energy band gap and hence the electronic properties in a wide range [16], just by controlling the oxide/nitride ratio.

In the present work, the electrical behavior of CrN_xO_y thin films, deposited by DC reactive magnetron sputtering, was investigated and correlated with their compositional and structural properties.

2. Experimental details

For the present work, CrN_xO_y films were deposited on glass and silicon (100) substrates by reactive DC magnetron sputtering, in a laboratory-sized deposition system. The deposition system is formed by two vertically opposed rectangular magnetrons (unbalanced of type 2), in a closed field configuration. The films were prepared with the substrate holder positioned at 70 mm from the target in all runs, using a DC current density of 75 A m^{-2} on the chromium target (99.6 at. %). Before each deposition the substrates were subjected to an etching process, using pure argon with a partial pressure of 0.3 Pa (70 sccm) and a pulsed current of 0.6 A (T_{on} = 1536 ns and f = 200 kHz) for 900 s.

A gas atmosphere composed of Ar + N_2+O_2 gas mixture (17:3 ratio) was used for the preparation of the all set of films. The Ar flow was kept constant at 60 sccm during all depositions. The mixed reactive gas flow (N_2+O_2) varied from 2 to 32 sccm (corresponding to a partial pressure variation between 1.0×10^{-2} and 2.5×10^{-1} Pa). The working pressure was approximately constant during the depositions (varying slightly between ~0.4 and 0.5 Pa). The substrates were grounded and a temperature close to 100 ºC was kept during the films deposition. The temperature evolution of the coated substrates (resulting from the deposition process itself) was monitored with a thermocouple placed close to the surface of the substrate holder. A delay time of five minutes was used before positioning the surface of the samples in front of the Cr target. This delay time was used to avoid film contaminations resulting from target poisoning from previous depositions and also to assure a practically constant deposition temperature of the substrates during film growth.

The atomic composition of the as-deposited samples was measured by Rutherford Backscattering Spectrometry (RBS) using either 1.4 or 1.75 MeV $^1H^+$ and 2 MeV $^4He^+$

beams. The scattering angles were 140º (standard detector, IBM geometry) and 180º (annular detector), tilt angles 0º and 30º. Composition profiles for the as-deposited samples were generated using the NDF [22] software. For the ^{14}N, ^{16}O and ^{28}Si data, the cross-sections given by Gurbich were used [23].

The crystallographic structure was investigated by X-ray diffraction (XRD), using a Philips PW 1710 diffractometer (Cu-Kα radiation) operating in a Bragg- Brentano configuration. XRD patterns were deconvoluted, assuming to be Pearson VII functions to yield the peak position, peak intensity and integral breadth [24].

The electrical resistivity of the conducting films was measured using the four-pointed probe method (in linear geometry) [25]. For high resistivity films, aluminum contacts (1×6 mm^2) were vapor deposited on the top of the coatings and the electrical resistivity of the films was obtained from the I-V characteristic.

3. Results and discussion

3.1. Deposition rate and film composition

Fig. 1 shows the evolution of the target potential and deposition rate as a function of the gas mixture (N_2+O_2) partial pressure. From the analysis of the target potential evolution with reactive gas pressure one can observe two major deposition regimes for the prepared samples. A first regime, with gas partial pressures between 0.01 and 0.1 Pa, characterized by relatively low target voltages with values around -380 V. The set of samples within this zone were prepared with reactive gas flows lower than 8 sccm, exhibiting metallic-like surface tones. A second zone follows, for partial gas pressures between 0.1 and 0.27 Pa, where the target voltage increased gradually from -375 V to values close to -420 V. Due to this variation of target voltage one would expect a gradual change in the growth modes of the samples within this zone as well as in its properties. This assumption was firstly confirmed by the sudden

modification in the surface appearance of the coatings within this second zone, which varied from metallic-like to interference-like ones.

To explain the behavior of the target voltage with the reactive gas pressure, one has to consider the gettering of the reactive gas by the target material, as shown by Berg et al. [26], leading to the formation of a compound layer on the target surface and thus affecting the reactive gas partial pressure and also the ion-induced secondary electron emission (ISEE) coefficient of the target material [27]. In this respect, it is widely known and accepted that the minimum voltage required to sustain the magnetron discharge is roughly inversely proportional to the γ_{ISEE} coefficient of the target material [28]. The dependence of this coefficient on the reactive gas partial pressure varies for different target materials and reactive gases, increasing for some metals like Al and Y, with increasing reactive gas incorporation on the target, while for Cr, Ti, Zr it decreases with the reactive gas incorporation [26]. In the present case, at low reactive gas flow, the reactive gas is almost completely gettered and hence the target condition remains metallic, which explains the low constant target voltage observed for the Cr target. On increasing the reactive gas flow, the amount of gas that can be gettered by the Cr target is reached, the reactive gas partial pressure increases and the target becomes gradually poisoned, which explains the steady increase in the target voltage observed for the set of samples that were indexed to the second zone.

Following the variation of target potential, the deposition rate measurements reveal again different types of films, confirming the analysis made above of the different film depositions. The evolution of deposition rate, Fig. 1b), indicates that the set of samples that were firstly divided into two major zones after the target potential analysis, should in fact be split into 3 different modes (regimes): i) a set of samples that were deposited within a metallic mode regime, which will be indexed from hereafter as zone I films; ii) a second set of samples that were deposited in an compound mode (oxide) regime, indexed from hereafter as zone II films;

and in between, a set of films that seem to have been deposited in a transition regime, which will be named zone T. The first regime – metallic mode, includes the group of samples prepared with reactive gas flows up to 8 sccm (corresponding to partial pressures varying from 0.01 to 0.1 Pa), revealing higher deposition rates (above 35 nm/min), which is characteristic of the sputtering process occurring in the metallic regime [29].

For reactive gas partial pressures above 0.16 Pa, there is a clear tendency for a progressive decrease of the deposition rate from roughly 40 nm/min to a value close to 10 nm/min at the highest reactive gas flow. The progressive decrease of the deposition rate within the oxide zone (zone II) is a consequence of the well-known poisoning effect of the target by both reactive gases [30]. Both chromium nitride and oxide layers form at the surface of the Cr target. Since the sputtering yield of both compounds is lower than that of Cr, a decrease in the deposition rate is expected. Between these two main zones (corresponding to the group of samples prepared with reactive gas flows between 12 and 20 sccm), one can clearly distinguish the previously mentioned transition zone, which maybe associated to the transition regime between the metallic and compound oxide regimes in the hysteresis cycle of pure nitrides, where the deposition rate tends to stabilize at about 40 nm/ min. The fact that the deposition rate does not change significantly makes the set of samples prepared within this growth mode share similar characteristics, namely in what concerns the morphology and structure, and thus their set of basic properties. The consistency in the deposition rate values suggests that the constant target potential values are responsible for an almost steady state of the sputtering process.

The evolution of deposition rate with the reactive gas flow is also well correlated with the change of the composition of the films and the correspondent ratios between the concentration of the different elements, shown in Figs. 2a) and b). Following the previous analysis, the samples in fig 2a) can be divided in the same three zones, which actually correspond to

important variations of the composition. Films in zone I, prepared with low partial pressure of reactive gas mixture ($p_{N2+O2} \leq 0.1$ Pa), reveal a chromium decrease from 75 at. % to a value close to 58 at. %, thus confirming the high sub-stoichiometric condition of these samples and their metallic nature, as was anticipated by their visual inspection. Oxygen and nitrogen present quite similar behaviors in this first zone, with the oxygen varying from about 13 to 21 at. %., and the nitrogen from around 11 to 21 at. %. For films prepared within zone T, the chromium content reveals a slight decrease from around 47at.% to a value close to 45 at. %. Oxygen and nitrogen contents are approximately constant and quite similar within this zone, at about 30 at. %. Regarding the samples prepared with the highest gas mixture partial pressures (between 0.16 to 0.25 Pa), zone II, the composition analysis, shown in Fig. 2a), again reveals the decrease of the chromium content from around 40 at.% to a value close to 32 at.%. The RBS analysis shows for this zone a slight decrease of the nitrogen content to around 8 at.% and a significant increase of the oxygen content from 43 at.% to a value close to 56 at.%.

Beyond these absolute values of composition and their variations, it is particularly important to notice the evolution of the atomic ratios of the different elements as shown in Fig. 2b), which may give the first indication about the particular tendency for compound formation. Within zone I, results show that all non-metals to chromium atomic ratios (C_O/C_{Cr}, C_N/C_{Cr} and C_{O+N}/C_{Cr}) have values below one, indicative of the sub-stoichiometric nature of the films, forming a kind of metastable solid solution of $Cr(N,O)_x$.

Within the transition zone, the C_O/C_{Cr} and C_N/C_{Cr} ratios are approximately constant, with values close to 0.6, while the C_{O+N}/C_{Cr} ratio is higher than 1, characteristic of an over-stoichiometric compound. On the other hand, the fact that the C_{O+N}/C_{Cr} ratio in this zone is still below 1.5 (the value that would correspond to the Cr_2O_3 compound) would mean, in a first approximation, that there is not enough oxygen (even if together with N) to form oxide-

like compounds (N-doped if this element could occupy some of the O positions within a $Cr_2(O,N)_3$-type compound). But at the same time it is also too high to form a oxygen-doped nitride-like phase. This may induce the possibility to have over-stoichiometric Cr(O,N)-type compound in this transition zone.

Finally, the films from zone II show an increase of the C_O/C_{Cr} and the C_{O+N}/C_{Cr} ratios to values around 1.7 and 2, respectively, with the C_N/C_{Cr} ratio decreasing to a value close to 0.3. This set of results can be explained by the higher binding enthalpy of chromium oxide (-564 kJ/mol per chromium atom) compared to chromium nitride (-125 kJ/mol), thus favouring the bonding of Cr atoms with oxygen [16]. The films from this zone are likely to be oxide-based Cr_2O_3 or CrO_2 compounds, with the excess of nitrogen probably being incorporated in lattice or in interstitial positions within the oxide phase [31,32].

3.2. Structural properties

Fig. 3 shows a summary of the different structural features revealed by the overall set of prepared samples. In fact, and following both the deposition characteristics (target potential and deposition rate) and composition analysis, the structural characterization revealed the development of three major types of crystalline structures, represented by each of the diffractograms depicted in Fig. 3. Thus, the set of samples that were prepared within the metallic-like zone I, represented in Fig. 3 by the sample prepared with the highest C_{O+N}/C_{Cr} ratio within this zone ($CrN_{0.36}$ $O_{0.37}$), showed the development of a very poorly crystallized structure (quasi-crystalline), where the position of the different diffraction patterns suggests some similarity to a fcc CrN-type. It is worth mentioning that a hcp Cr-type phase may also be present as evidenced by the large and broad peak at around $2\theta = 44^o$ as well as the peak tail at $2\theta \approx 65^o$, meaning that the samples in this zone probably consist of a mixture of both CrN(O) and Cr(O) phases. The presence of (O) here takes into account the non-negligible

possibility that it may be incorporated in both structures [31,32]. Notice also the relatively high shift in the peak positions for the CrN(O) phase, which can be easily understood taking into account the sub-stoichiometric condition of the samples in this zone (C_O/C_{Cr} and C_N/C_{Cr} below 0.4 and C_{O+N}/C_{Cr} ratio below 0.7), and the fact that oxygen, being very reactive, may be occupying nitrogen positions in the CrN lattice (as mentioned above), thus inducing significant lattice distortions.

Regarding the samples from zone T, Fig. 3 clearly shows that a CrN-type structure is present, with relatively high crystallinity, as demonstrated by the XRD pattern of the $CrN_{0.71}O_{0.65}$ sample. The two diffraction peaks observed correspond to (111) and (200) planes of that fcc CrN(O)-type structure, with a (111) preferential growth. As already anticipated by the composition analysis no oxide phase is observed which may be easily understood by the insufficient oxygen content in the films to form such a Cr_2O_3 phase. It is also important to note the much higher crystallinity of these samples when compared to the results obtained for the zone I samples. Furthermore, it is also worth to note the significantly lower shift in the peaks position compared to those of zone I. The main reason for such behavior is certainly associated with the particular stoichiometry of the samples within this zone. As demonstrated in Fig. 2 the samples prepared within zone T have C_O/C_{Cr} and C_N/C_{Cr} ratios close to 0.6, while the C_{O+N}/C_{Cr} ratio varies between about 1 and 1.3. Taking into account the possibility to have O occupying N positions within the fcc CrN lattice (quite probable due to the low C_N/C_{Cr} ratio), this would lead to an increasing stoichiometric condition of the crystalline phase and thus to a continuous approach towards the CrN peak positions.

Finally the samples prepared within zone II, reveal structural features are clearly different from the samples of the two previous zones, as shown in the diffractogram of the sample with composition $CrN_{0.25}O_{1.64}$, developing an amorphous-type structure that may correspond to a oxide-like phase, as demonstrated by R. Mientus et al. [16].

3.3. Electrical resistivity

The electrical resistivity of the samples is plotted in Fig. 4 as a function of the non-metallic/metallic chemical ratio, C_{O+N}/C_{Cr}. Regarding the samples from zone I, which presented a sub-stoichiometric condition and a poorly crystallized fcc CrN-type structure, the resistivity analysis revealed relatively low values of resistivity, from 7.2×10^2 μΩ cm to around 1.5×10^3 μΩ cm, which are characteristic of metallic-like compounds. The values are relatively close to those of chromium nitride with varied stoichiometries, CrN_x ($1\times10^2 < \rho_{CrNx} < 15\times10^4$ μΩ cm) [33]. Furthermore, Mientus et al. [16] reported resistivity values of CrON films in the vicinity of 1×10^4 μΩ cm for the lower nitride range in nitride-based coatings, the equivalent to zone I in this paper. In any case, one must keep in mind that their coatings were already in the stoiciometric condition, and thus the range did not include the entire set of sub-stoichiometric nitride compositions (O doped), which in the present case explains the variation from 1×10^2 to 1×10^4 μΩ cm.

For the samples prepared within the transition zone, where the composition analyses revealed a C_{O+N}/C_{Cr} ratio increase to an over-stochiometric condition and the structural analysis showed a highly crystalline fcc CrN-type phase, the resistivity analysis reveals an increase of the electrical resistivity of the films with values ranging between 7×10^3 and 1.4×10^5 μΩ cm. Again, there is a good agreement between these results and those obtained for both the CrN_x and CrO_xN_y systems [33]. The first important note is the good agreement between the results obtained for the films within this transition zone and those obtained by R. Mientus et al. [16], which have quite similar values in their stoichiometric to close-stoiciometric-like CrO_xN_y films. It is also important to note the agreement of the resistivity values of the samples from zone T with those of bulk chromium nitride ($\rho_{CrN} = 1\times10^4$ Ω cm) [16].

Finally, the oxide-like samples prepared within zone II presented, as expected, insulator-type behavior with high values of resistivity varying between 1.9×10^{7} and 1.1×10^{9} $\mu\Omega$ cm, consistent with Cr_2O_3 resistivity ($\rho_{Cr2O3} >> 10^{8}$ $\mu\Omega$ cm) and far beyond the values obtained in zone T. This increase in the resistivity is also consistent with the increase in the stoichiometry of the samples, Fig. 2, especially that of C_O/C_{Cr}, which goes even beyond that of Cr_2O_3.

4. Conclusion

Chromium oxynitride films CrN_xO_y were prepared by reactive DC magnetron sputtering using a chromium target and a gas mixture composed of argon and a reactive mixture of oxygen + nitrogen (3:17 atomic ratio). From the evolution of the target voltage and deposition rate as a function of the partial pressure of reactive gas mixture three different types of films were found: metallic like films (Zone I), oxide like ones (Zone II) and a transition zone (Zone T) between them. The films in Zone I were prepared with low values of partial pressure and high deposition rates, with the composition, structural and electrical characterization revealing sub-stoichiometric films with a quasi-crystalline CrN- type compounds and low electrical resistivity values. The films from Zone T, corresponding to intermediate reactive gas partial pressures, reveal an over-stoichiometric character and fcc structure (CrN) with relatively high degree of crystallinity and electrical resistivity values comparable to those of Zone I. Finally the films prepared with high partial pressures of reactive gas, that is, Zone II (oxide zone) semi-transparent films, present an over-stochiometric oxide like character with an amorphous-type structure and high values of electrical resistivity consistent with insulator behavior. This work suggests that by simply changing the reactive gas flow it is possible to tune the electrical properties of CrNO compounds in a wide range, from metallic like to semiconducting behaviour.

References

[1]. H. K. Pulker, Coatings on Glass, Thin Films Science and Technology Vol. 6, Elsevier, (Amsterdam, 1984).

[2]. H. Bach, N. Neuroth, The properties of Optical Glass, Springer, (Heidelberg 1995).

[3]. N. Martin, A. Besnard, F. Sthal, F. Vaz, C. Nouveau, The contribution of grain boundary barriers to the electrical conductivity of titanium oxide thin films, Applied Physics Letters 93 (2008) 064102.

[4]. S.T. Oyama, Chemistry of Transition Metal Carbides and Nitrides, Blackie Academic & Professional, (New York, 1996).

[5]. J.-L. Calais, Band structure of transition metal compounds, Adv. Phys. 26 (1977) 847-885.

[6]. K. Schwarz, Band structure and chemical bonding in transition metal carbides and nitrides, CRC Crit. Rev. Solid State Mater. Sci. 13 (1987) 211-257.

[7]. P. Carvalho, J. M. Chappé, L. Cunha, S. Lanceros-Méndez, P. Alpuim, F. Vaz, E. Alves, C. Rousselot, J. P. Espinós, and A. R. González-Elipe, Influence of the chemical and electronic structure on the electrical behaviour of zirconium oxynitride films, J. Appl. Phys. 103 (2008) 104907.

[8]. N. Martin, O. Banakh, A. M. E. Santo, S. Springer, R. Sanjinés, J. Takadoum, F. Lévy, Reactive sputtering of TiO_xN_y coatings by the reactive gas pulsing process. Part I: Pattern and period of pulses, App. Surf. Sci. 185 (2001) 123-133.

[9]. M. Fenker, H. Kappl, O. Banakh, N. Martin, J.F. Pierson, Investigation of Niobium oxynitride thin films deposited by reactive magnetron sputtering, Surf. Coat. Technol. 201 (2006) 4152-4157.

[10]. H. Le Dréo, O. Banakh, H. Keppner, P.-A. Steinmann, D. Briand, N.F. de Rooij, Optical, electrical and mechanical properties of the tantalum oxynitride thin films deposited by pulsing reactive gas sputtering, Thin Solid Films 515 (2006) 952-956.

[11]. C. Petitjean, M. Grafouté, C. Rousselot, J.F. Pierson, Reactive gas pulsing process, A method to extend the composition range in sputtered iron oxynitride films, Surf. Coat. Technol. 202 (2008) 4825-4829.

[12]. N.M.G. Parreira, N.J.M. Carvalho, F. Vaz, A. Cavaleiro, Mechanical evaluation of unbiased W–O–N coatings deposited by d.c. reactive magnetron sputtering, Surf. Coat. Technol. 200 (2006) 6511-6516

[13]. B. Gakovic, M. Trtica, P. Panjan, M. Cekada, Surface modification of the Cr-based coatings by the pulsed TEA CO_2 laser, Appl. Phys. A 79, (2004) 1353-1355.

[14]. Y. Shi, S. Long, L. Fang, S. Yang, F. Pan, Effect of nitrogen content on the properties of $CrN_xO_yC_z$ coating prepared by DC reactive magnetron sputtering, Appl. Surf. Sci. 254 (2008) 5861-5867.

[15]. S. Agouram, F. Bodart, G. Terwagne, Characterisation of reactive unbalanced magnetron sputtered chromium oxynitride thin films with air, Surf. Coat. Technol. 180–181 (2004) 164-168.

[16]. R. Mientus, R. Grotschel, K. Ellmer, Optical and electronic properties of CrO_xN_y films deposited by reactive DC magnetron sputtering in $Ar/N_2/O_2(N_2O)$ atmospheres, Surf. Coat. Technol. 200 (2005) 341-345.

[17]. T. Suzuki, H. Saito, M. Hirai, H. Suematsu, W. Jiang, K. Yatsui, Preparation of $Cr(N_x,O_y)$ thin films by pulsed laser deposition, Thin Solid Films 407 (2002) 118-121.

[18]. V. Ezirmik, E. Senel, K. Kazmanli, A. Erdemir, M. Ürgen, Effect of copper addition on the temperature dependent reciprocating wear behaviour of CrN coatings, Surf. Coat. Technol. 202 (2007) 866-870.

[19]. X. Pang, K. Gao, F. Luo, H. Yang, L. Qiao, Y. Wang, A.A. Volinsky, Annealing effects on microstructure and mechanical properties of chromium oxide coatings, Thin Solid Films 516 (2008) 4685-4689.

[20]. M.F. Al-Kuhaili, S.M.A. Durrani, Optical properties of chromium oxide thin films deposited by electron-beam evaporation, Optical Materials 29 (2007) 709-713.

[21]. N. Popovici, M.L. Paramês, R.C. Silva, O. Monnerea, P.M. Sousal, A.J. Silvestre, O. Conde, KrF pulsed laser deposition of chromium oxide thin films from Cr_8O_{21} targets, Appl. Phys. A 79, (2004) 1409-1411.

[22]. N.P. Barradas, C. Jeynes, M.A. Harry, RBS/simulated annealing analysis of iron-cobalt silicides, Nucl. Instr. and Meth. B 136 (1998) 1163.

[23]. A. F. Gurbich, Evaluated differential cross-sections for IBA, Nucl. Instr. and Meth. B 268 (2010) 1703.

[24]. I. Horcas, R. Fernandez, J.M. Gomez-Rodriguez, J. Colchero, J.G. Herrero, A.M. Baro, WSXM: A software for scanning probe microscopy and a tool for nanotechnology, Rev. Sci. Inst. 78 (2007) 013705.

[25]. A.W. Robert, An algorithm for computing linear four-point probe thickness correction factor, Rev.of Sci. Inst. 72 (2001) 3580-3586.

[26]. D. Depla, S. Mahieu, Reactive sputter deposition, Springer (2008).

[27]. D.A. Glocker, S.I. Shah, Thin Film Process Technology, edited by Institute of Physics Publising Ltd, (Bristol, UK, 1995).

[28]. J. Borges, F. Vaz, L. Marques, AlNxOy thin films deposited by dc reactive magnetron sputtering, Appl. Surf. Sci. 257 (2010) 1478.

[29]. F. Vaz, P. Carvalho, L. Cunha, L. Rebouta, C. Moura, E. Alves, A.R. Ramos, A. Cavaleiro, Ph. Goudeau, J.P. Rivière, Property change in ZrN_xOy thin films: effect of the oxygen fraction and bias voltage, Thin Solid Films 469-470 (2004) 11.

[30]. M. Ohring, The Materials Science of Thin Films, edited by Academic Press, (New York, 1992).

[31]. P. Carvalho, F. Vaz, L. Rebouta, L. Cunha, C. J. Tavares, C. Moura, E. Alves, A. Cavaleiro, Ph. Goudeau, E. Le Bourhis, J. P. Rivière, J. F. Pierson, O. Banakh, Structural, electrical, optical, and mechanical characterizations of decorative ZrO_xN_y thin films, J. Appl. Phys. 98 (2005), 023715.

[32]. P. Carvalho, J. M. Chappé, L. Cunha, S. Lanceros-Méndez, P. Alpuim, F. Vaz, E. Alves, C. Rousselot, J.P. Espinós, and A.R. González-Elipe, Influence of the chemical and electronic structure on the electrical behavior of zirconium oxynitride films, J. Appl. Phys. 103 (2008) 104907

[33]. E. Ando, S. Suzuki, Optical and mechanical properties of Cr and CrN_x films by dc magnetron sputtering, Journal of Non-Crystalline Solids 218 (1997) 68-73.

FIGURE CAPTIONS

Fig.1 a) Evolution of the target potential and deposition rate b**)** as a function of the partial pressure of reactive gas (N_2+O_2). The pressure was measured prior to discharge ignition.

Fig. 2. Evolution of the: (a) chemical composition and (b) concentration ratio as a function of the partial pressure of reactive gas (N_2+O_2). The pressure was measured prior to discharge ignition. The chemical composition of all samples was determined within an error of about 3-5 at. %.

Fig. 3. X-ray diffraction patterns for representative samples of each of the three identified zones with different crystallographic features.

Fig. 4. Electrical resistivity at room temperature of the films as a function of the C_{O+N}/C_{Cr} concentration ratio.

Figure 1 a)

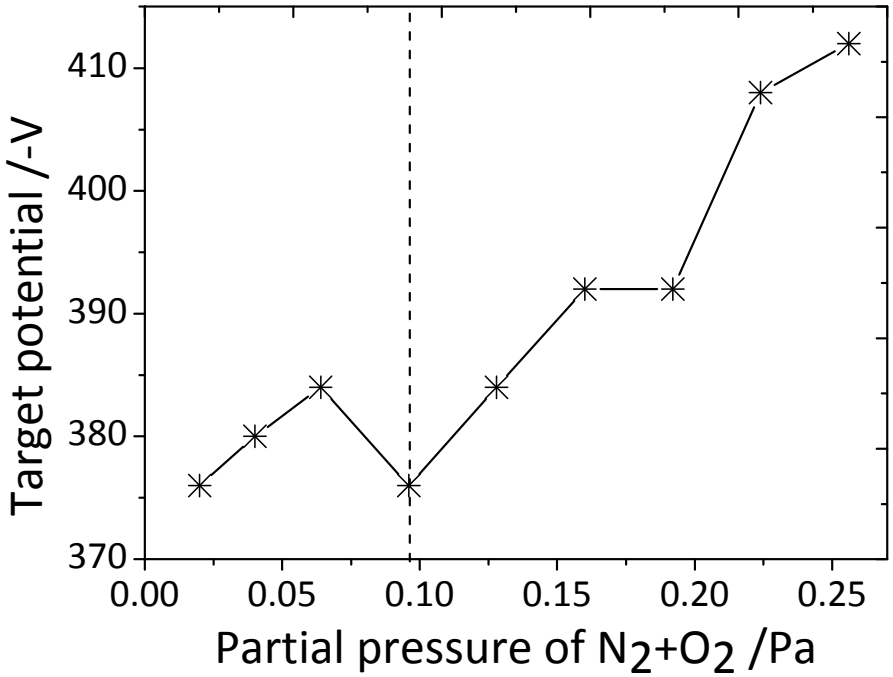

Figure 1 b)

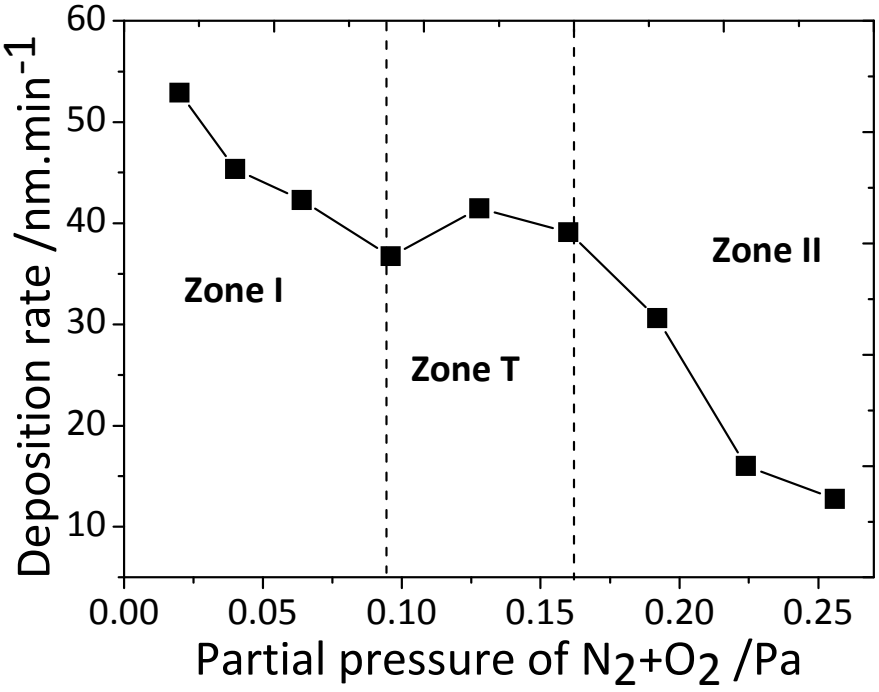

Figure 2 a)

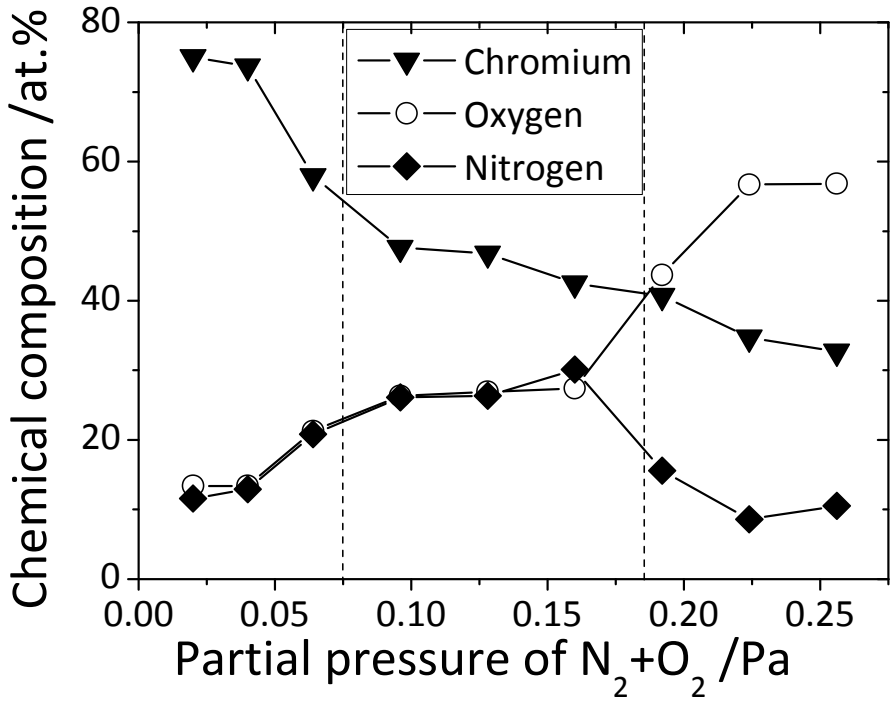

Figure 2 b)

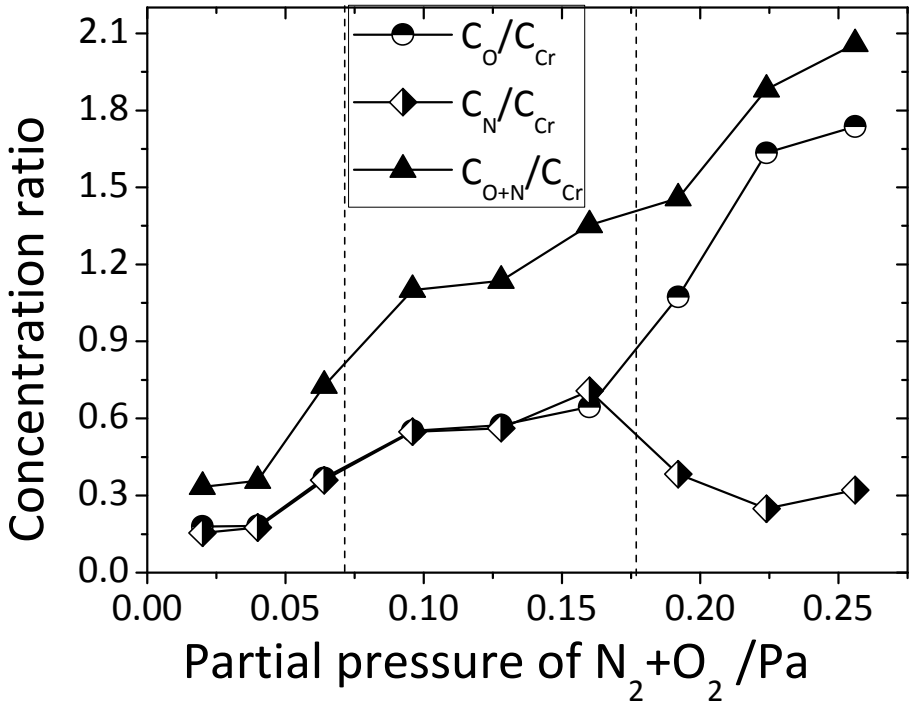

Figure 3

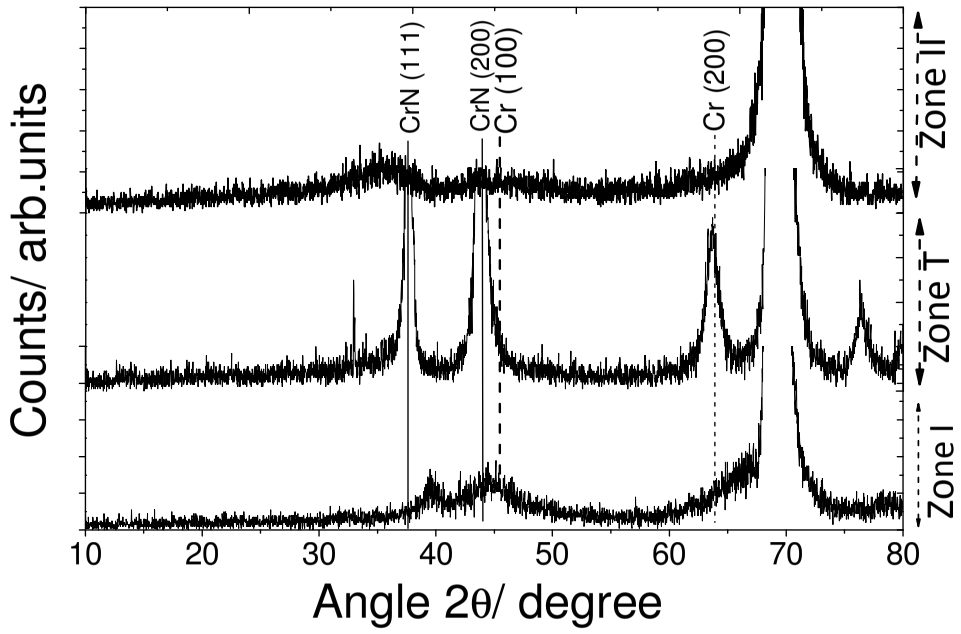
Counts/ arb.units
CrN (111)
CrN (200)
Cr (100)
Cr (200)
Zone II
Zone T
Zone I
10
20
30
40
50
60
70
80
Angle 2θ/ degree

Figure 4

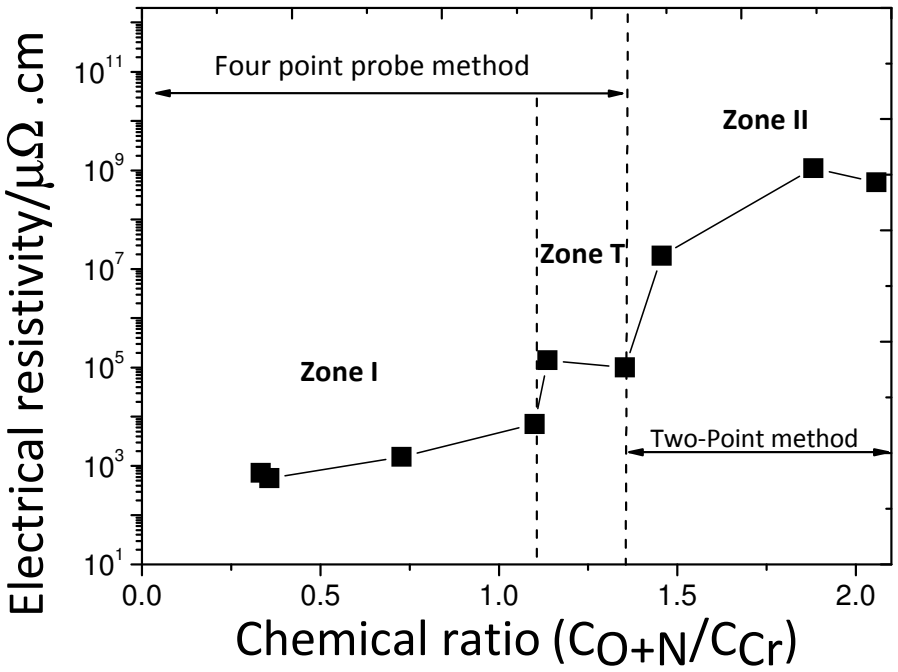
Four point probe method
Zone II
Zone T
Zone I
Two-Point method
Electrical resistivity/μΩ .cm
Chemical ratio (C_{O+N}/C_{Cr})
10^{11}
10^{9}
10^{7}
10^{5}
10^{3}
10^{1}
0.0
0.5
1.0
1.5
2.0